Diffusiophoresis of a Charge-Regulated Sphere along the Axis of an Uncharged Cylindrical Pore

ARTICLE *in* LANGMUIR · FEBRUARY 2010

Impact Factor: 4.46 · DOI: 10.1021/la904726k · Source: PubMed

3 AUTHORS, INCLUDING:

Wei-Lun Hsu
The University of Tokyo
17 PUBLICATIONS **128** CITATIONS

Diffusiophoresis of a Charge-Regulated Spherical Particle Normal to Two Parallel Disks

Jyh-Ping Hsu,* Kuan-Liang Liu, Wei-Lun Hsu, and Li-Hsien Yeh

Department of Chemical Engineering, National Taiwan University, Taipei, Taiwan 10617

Shiojenn Tseng

Department of Mathematics, Tamkang University, Tamsui, Taipei, Taiwan 25137

Received: August 10, 2009; Revised Manuscript Received: January 14, 2010

The diffusiophoresis of a charge-regulated spherical particle normal to two parallel disks as a response to an applied uniform electrolyte concentration gradient is modeled theoretically. The fixed charge on the particle surface comes from the dissociation/association reactions of the functional groups, yielding a charge-regulated surface, which simulates biological cells. Numerical simulations are conducted to examine the behavior of a particle under various conditions: the parameters considered in the simulation include the thickness of the double layer, the charged conditions on the particle surface, the relative size of the particle, and the particle−disk distance. Because the diffusiophoretic mobility of a particle can be dominated by chemiphoresis, electrophoresis, or osmotic flow, the diffusiophoretic behavior of the particle is complicated. For instance, the diffusiophoretic mobility may have two local maximums and a local minimum as the thickness of the double layer varies. This behavior is of practical significance if diffusiophoresis is adopted as a separation operation or as a tool to characterize the surface properties of a particle.

1. Introduction

Charged colloidal particles suspended in a solution can be driven by an applied concentration gradient, known as diffusiophoresis.[1] The driving force in this phenomenon depends upon the nature of the solutes, which can be electrolytes[2] or nonelectrolytes.[3] Compared with electrophoresis, in which a charged particle is driven by an applied electric field, diffusiophoresis has the advantage of no Joule heat effect[4] and, therefore, has the potential to be used as an analytical tool to characterize the charged conditions of a particle or as a separation/purification operation.[5−9] In biological systems, the liquid phase is usually of ionic nature. In this case, the diffusiophoresis of a particle is driven mainly by chemiphoresis[10] and electrophoresis.[11,12]

Chemiphoresis comes from the double-layer polarization (DLP) induced by the interaction between the particle and the applied concentration gradient. Two types of DLP are identified: type I DLP drives a particle toward the high-concentration side, and type II DLP drives a particle toward the low-concentration side.[13−16] If the diffusivity of cations and that of anions are the same, such as in an aqueous potassium chloride solution, a charged particle is driven solely by chemiphoresis.

Electrophoresis comes from an induced electric field, which arises from the difference between the diffusivity of cations and that of anions. In an aqueous sodium chloride solution, for example, because the diffusivity of Cl^- is larger than that of Na^+, the diffusion of these two types of ions yields a local electric field. Because the direction of this electric field points to the low-concentration side, a positively charged particle is driven toward that direction.[16] Note that because chemiphoresis is also present in such a system, the direction of diffusiophoresis depends upon the net result of the competition between chemiphoresis and electrophoresis. The presence of these two effects was justified experimentally by Ebel et al.[10]

Compared with those for the case in which a particle is driven by an applied electric field, the available theoretical results for diffusiophoresis are very limited. Adopting a unit cell model, Wei and Keh[17] solved analytically the diffusiophoresis of a suspension of particles for the case of low surface potential and arbitrary double-layer thickness. Lou et al.[18] extended their analysis to the case of arbitrary surface potential. Several attempts had been made on the assessment of the presence of a boundary on the diffusiophoretic behavior of a particle. Lou and Lee, for example, considered the diffusiophoresis of a charged spherical particle normal to a plane.[19] The diffusiophoresis of a charged spherical particle along a cylindrical pore was studied by Keh and Hsu.[20] Chang and Keh[21] analyzed the diffusiophoresis of a charged spherical particle normal to two planar parallel walls. Hsu et al.[16] investigated the diffusiophoresis of a charged particle in a spherical cavity. In general, the presence of a boundary was shown to have a significant influence, both qualitatively and quantitatively, on the diffusiophoretic behavior of a particle.

Intuitively, the charged conditions on the surface of a particle play a significant role in its diffusiophoresis. Available results in the literature almost always assume that the particle surface is maintained at either constant potential or constant charge density. These constant surface property models are idealized ones representing limiting cases of a more general model on the particle surface, known as the charge-regulated surface model.[22] In practice, using the constant surface property models can be unrealistic in cases such as cells and platelets[23] and particles covered by an artificial membrane.[24,25] Keh and Li[26] analyzed the diffusiophoresis of a dispersion of charge-regulated spherical particles at low surface potentials.

In this study, we consider the diffusiophoresis of a charge-regulated spherical particle at an arbitrary position between two large, parallel disks normal to these disks. The problem considered allows us to examine the boundary effect on diffusiophoresis for the case that the particle surface assumes a general

* Corresponding author. Phone: 886-2-23637448. Fax: 886-2-23623040. E-mail: jphsu@ntu.edu.tw.

10.1021/jp907696t
Published on Web 02/09/2010

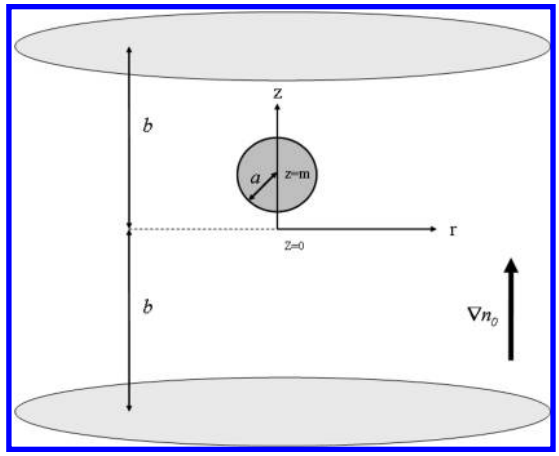

Figure 1. Diffusiophoresis of a rigid spherical particle of radius a in an electrolyte solution as a response to a uniform applied concentration field, ∇n_0, normal to two large parallel disks with half separation distance, b. (r, θ, z) are the cylindrical coordinates with its origin at the center between the two disks, ∇n_0 is in the z-direction, and the center of the particle is at $z = m$.

charged condition. Both the effect of chemiphoresis and electrophoresis are taken into account in the analysis. Numerical simulations are conducted to examine in detail the influences of the key factors, including the position and the size of a particle, the thickness of double layer, the charged conditions on the particle surface, and the difference in the diffusivity of cations and that of anions on the diffusiophoretic behavior of the particle.

2. Theory

As illustrated in Figure 1, we consider the diffusiophoresis of a spherical particle of radius a in an electrolyte solution as a response to a uniform applied concentration field, ∇n_0, normal to two large parallel disks with half separation distance, b. (r, θ, z) are the cylindrical coordinates with its origin at the center between two disks, ∇n_0 is in the z-direction, and the center of the particle is at $z = m$. Both the particle and the disks are rigid and nonconductive, and the solution contains z_1/z_2 electrolytes. Let $\alpha = -z_2/z_1$. Note that the geometry chosen is θ-symmetric, and therefore, only the (r, z) domain needs be considered.

The governing equations of the present problem include those for the electric, the concentration, and the flow fields, and can be summarized as the following:[27]

$$\nabla^2\psi = -\frac{\rho}{\varepsilon} = -\sum_1^2 \frac{z_j e n_j}{\varepsilon} \tag{1}$$

$$\nabla\cdot\left[-D_j\left(\nabla n_j + \frac{z_j e}{k_B T} n_j \nabla\psi\right) + n_j\mathbf{u}\right] = 0 \tag{2}$$

$$\nabla\cdot\mathbf{u} = 0 \tag{3}$$

$$-\nabla p + \eta\nabla^2\mathbf{u} - \rho_e\nabla\psi = 0 \tag{4}$$

Here, ψ, p, and ρ are the electric potential, the pressure, and the space charge density respectively; ε, η, and $\mathbf{u}$ are the permittivity, viscosity, and velocity of the liquid phase, respectively; e, k_B, and T are the elementary charge, Boltzmann constant, and the absolute temperature, respectively; and z_j, D_j, and n_j are the valence, diffusivity, and number concentration of ion species j, respectively. The subscripts 0, 1, and 2 refer to the bulk property, cations, and anions, respectively; and ∇ and ∇^2 are the gradient operator and the Laplace operator, respectively. Suppose that the applied concentration field is weak so that the double layer surrounding the particle is only slightly distorted when ∇n_0 is applied, that is, $a|\nabla n_0| \ll n_{0e}$, where n_{0e} is the bulk solute concentration at equilibrium. Under this condition, p, ψ, n_j, and $\mathbf{u}$ can all be decomposed into an equilibrium term arising from the presence of the particle and the disks and a perturbed term arising from the application of ∇n_0.[28] Using subscript e and prefix δ to denote the equilibrium and the perturbed terms, respectively, we have

$$p = p_e + \delta p \tag{5}$$

$$\psi = \psi_e + \delta\psi \tag{6}$$

$$n_j = n_{je} + \delta n_j \tag{7}$$

$$\mathbf{u} = \mathbf{u}_e + \delta\mathbf{u} \tag{8}$$

Because the particle is stagnant when ∇n_0 is not applied, $\mathbf{u}_e = 0$. It can be shown that the equilibrium concentration of each ionic species follows a Boltzmann distribution, $n_j = n_{j0}\exp[-(z_j e\psi_e)/k_B T]$.[29] We assume that the perturbed electrochemical potential energy, $\delta\mu_j$, can be expressed as a linear combination of δn_j and $\delta\psi$,[26]

$$\delta\mu_j = k_B T\frac{\delta n_j}{n_{je}} + z_j e\,\delta\psi \tag{9}$$

It can be shown that under the condition of weak applied concentration gradient, eqs 1, 2, and 4−9 lead to the following scaled equations:[27,28,30]

$$\nabla^{*2}\psi_e^* = -\frac{(\kappa a)^2}{1+\alpha}[\exp(-\psi_e^*) - \exp(\alpha\psi_e^*)] \tag{10}$$

$$\nabla^{*2}\,\delta\psi^* - \frac{(\kappa a)^2}{1+\alpha}[\exp(-\psi_e^*) + \alpha\exp(\alpha\psi_e^*)]\delta\psi^* = -\frac{(\kappa a)^2}{1+\alpha}[\exp(-\psi_e^*)\delta\mu_1^* - \alpha\exp(\alpha\psi_e^*)\delta\mu_2^*] \tag{11}$$

$$\nabla^{*2}\,\delta\mu_1^* = \nabla^*\psi_e^*\cdot\nabla^*\,\delta\mu_1^* - \gamma Pe_1\mathbf{u}^*\cdot\nabla^*\psi_e^* \tag{12}$$

$$\nabla^{*2}\,\delta\mu_2^* = -\alpha[\nabla^*\psi_e^*\cdot\nabla^*\,\delta\mu_2^* - \gamma Pe_2\mathbf{u}^*\cdot\nabla^*\psi_e^*] \tag{13}$$

$$n_1^* = \exp(-\psi_e^*)[1 + \delta\mu_1^* - \delta\psi^*] \tag{14}$$

$$n_2^* = \exp(\alpha\psi_e^*)[1 + \delta\mu_2^* + \alpha\,\delta\psi^*] \tag{15}$$

Here, $\nabla^* = a\nabla$, $\nabla^{*2} = a^2\nabla^2$, $\psi_e^* = \psi_e/\zeta$, $\delta\psi^* = \delta\psi/\zeta$, $\delta\mu_j^* = \delta\mu_j/k_B T$, $\gamma = \nabla^* n_0^*$, $\kappa^2 = \sum_{j=1}^2[n_{j0e}(ez_j)^2/\varepsilon k_B T]$, $Pe_j = \varepsilon(k_B T/ez_1)^2/\eta D_j$, $n_0^* = n_0/n_{j0e}$, $n_j^* = n_j/n_{j0e}$, and $\mathbf{u}^* = \mathbf{u}/U_{ref}$. Pe_j and κ are the electric Peclet number of ionic species j and the

reciprocal Debye length, respectively; $\zeta = k_B T/ez_1$; $U_{ref} = \varepsilon\gamma(k_B T/ez_1)^2/a\eta$ is a reference velocity.

In terms of the scaled symbols, the flow field can be described by[31]

$$\nabla^* \cdot \mathbf{u}^* = 0 \tag{16}$$

$$-\nabla^* \delta p^* + \gamma \nabla^{*2} \mathbf{u}^* + \nabla^{*2} \psi_e^* \nabla^* \delta\psi^* + \nabla^{*2} \delta\psi^* \nabla \psi_e^* = 0 \tag{17}$$

where $\delta p^* = \delta p/p_{ref}$, $p_{ref} = \varepsilon\zeta^2/a^2$ being a reference pressure.

Suppose that the particle surface is of charge-regulated nature. To simulate this, we assume that the particle surface contains both acidic functional groups, Q_AH, and basic functional groups, Q_B. The dissociation/association reactions of these functional groups can be expressed by[32]

$$Q_AH \leftrightarrow Q_A^- + H^+ \tag{18}$$

$$Q_BH^+ \leftrightarrow Q_B + H^+ \tag{19}$$

If we let K_A and K_B be the equilibrium constant of the dissociation/association reactions of Q_AH and Q_B, respectively, then

$$K_A = \frac{[Q_A^-]_s[H^+]_s}{[Q_AH]_s} \tag{20}$$

$$K_B = \frac{[Q_B]_s[H^+]_s}{[Q_BH^+]_s} \tag{21}$$

Here, subscript s denotes surface properties, and $[Q_A^-]_s$, $[Q_AH]_s$, $[Q_B]_s$, and $[Q_BH^+]_s$ are the number concentrations of Q_A^-, Q_AH, Q_B, and Q_BH^+ per unit surface area of the particle, respectively. $[H^+]_s$ is the concentration of H^+ on the particle surface. Suppose that the spatial distribution of H^+ follows Boltzmann distribution, $[H^+]_s = [H^+]_0 \exp(-\psi_e^*)$,[33] where $[H^+]_0$ is the bulk concentration of H^+. If we let N_A and N_B be the total number concentrations of Q_AH and Q_B per unit surface area, respectively, and σ_p be surface charge density, then

$$N_A = [Q_AH]_s + [Q_A^-]_s \tag{22}$$

$$N_B = [Q_BH^+]_s + [Q_B]_s \tag{23}$$

$$\sigma_p = e([Q_A^-H^+]_s - [Q_A^-]_s) \tag{24}$$

Equations 20−24 and the Boltzmann distribution of H^+ yield

$$\sigma_p^* = \frac{\theta AB \exp(-\zeta_p)}{\omega[1 + \theta B \exp(-\zeta_p)]} - \frac{A}{1 + B\exp(-\zeta_p)} \quad \text{on the particle surface} \tag{25}$$

where $\sigma_p^* = \sigma_p a/\varepsilon\xi$ is the scaled surface charge density, and ζ_p is the scaled surface potential of the particle. $A = e^2 N_A a/\varepsilon k_B T$, $B = [H^+]_s/K_A$, $\omega = N_A/N_B$, and $\theta = K_A/K_B$. Applying the Gauss law,[31] eq 25 leads to the following boundary condition:

$$\mathbf{n} \cdot \nabla^* \psi_e^* = -\frac{\theta AB \exp(-\zeta_p)}{\omega[1 + \theta B \exp(-\zeta_p)]} + \frac{A}{1 + B\exp(-\zeta_p)} \quad \text{on the particle surface} \tag{26}$$

where $\mathbf{n}$ is the unit normal vector direct into the liquid phase.

If both the particle and the disks are nonconductive, nonslip, and impermeable to ionic species, the concentration of ionic species reaches the bulk value, and the net charge flux vanishes on the disk surface.[16,19,21] Then the other boundary conditions associated with eqs 10−17 can be expressed as[34,35]

$$\psi_e^* = 0 \quad \text{on the disk surface} \tag{27}$$

$$\psi_e^* = 0 \quad \text{as } r \to \infty \tag{28}$$

$$\mathbf{n} \cdot \nabla^* \delta\psi^* = 0 \quad \text{on the particle surface} \tag{29}$$

$$\mathbf{n} \cdot \nabla^* \delta\psi^* = \beta\gamma \quad \text{on the upper disk surface} \tag{30}$$

$$\mathbf{n} \cdot \nabla^* \delta\psi^* = -\beta\gamma \quad \text{on the lower disk surface} \tag{31}$$

$$\mathbf{n} \cdot \nabla^* \delta\psi^* = 0 \quad \text{as } r \to \infty \tag{32}$$

$$\mathbf{n} \cdot \nabla^* \delta\mu_j^* = 0 \quad \text{on the particle surface} \tag{33}$$

$$\delta\mu_1^* = z^*\gamma + \delta\psi^* \quad \text{on the disk surface or as } r \to \infty \tag{34}$$

$$\delta\mu_2^* = z^*\gamma - \alpha\,\delta\psi^* \quad \text{on the disk surface or as } r \to \infty \tag{35}$$

$$\mathbf{u}^* = U^* \mathbf{e}_z \quad \text{on the particle surface} \tag{36}$$

$$\mathbf{u}^* = 0 \quad \text{on the disk surface or as } r \to \infty \tag{37}$$

Here, $z^* = z/a$, $\beta = (D_1 - D_2)/(D_1 + \alpha D_2)$, and $\mathbf{e}_z$ is the unit vector in the z-direction. $U^* = U/U_{ref}$, where U is the velocity of the particle.

Instead of solving directly the governing equations subject to the boundary conditions assumed, the original problem is partitioned into two subproblems:[16] (a) the particle moves with a constant velocity U in the absence of ∇n_0; and (b) ∇n_0 is applied, but the particle is fixed. Let $\mathbf{F}_i$ be the total force acting on the particle in subproblem i, $i = 1, 2$, and F_i be its magnitude. Then, $F_1 = C_1 U$ and $F_2 = C_2 \nabla n_0$, where the constant C_1 is related to a, η, and the particle−disk distance, but is independent of U,[35] and the constant C_2 is independent of ∇n_0.[10] Assuming that the system is at pseudo steady state condition, $F_1 + F_2 = 0$, which yields

$$U = -\frac{C_2}{C_1} \nabla n_0 \tag{38}$$

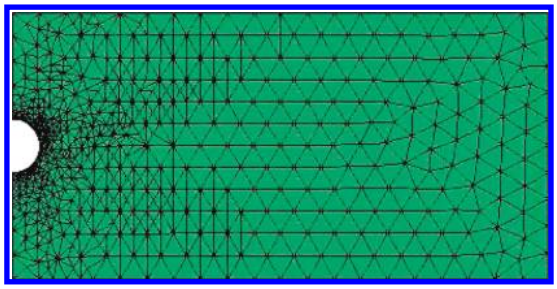

Figure 2. Typical mesh structure generated by FlexPDE on the half plane $\theta = \pi/2$ where the number of nodes is 5569.

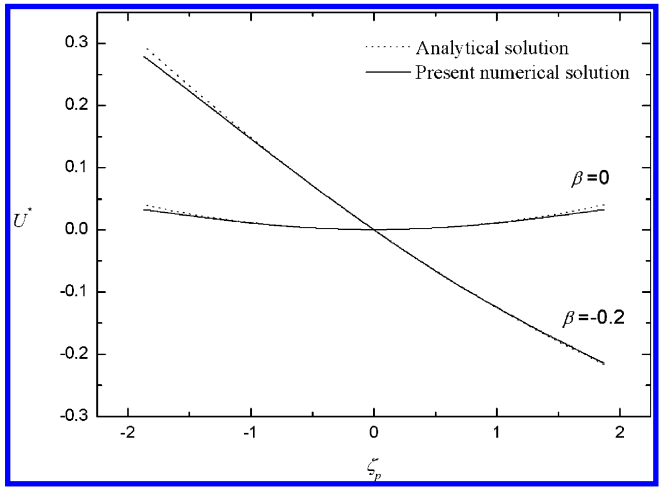

Figure 3. Variation of the scaled diffusiophoresis mobility, U^*, as a function of the scaled surface potential ζ_p. Solid curve: present numerical results at $\kappa a = 1$ and $\lambda = 0.1$, the values of ζ_p are obtained by varying the values of A and B. Dashed curve: analytical results for the case of an isolated rigid sphere.[37]

TABLE 1: Comparison of the Present Theoretical Results with the Experiment Data of Ebel et al.[10]

	KCl solution			
κa	4.2	6	11	18
ζ_p	−4	−3.2	−3.3	−4.2
U^* (theor)	0.112	0.17	0.262	0.512
U^* (exptl)	0.126	0.187	0.293	0.54
% deviation	−11.1	−9.1	−10.6	−5.2
	NaCl solution			
κa	3.9	6	11	18
ζ_p	−4	−3.05	−3	−3.6
U^* (theor)	0.412	0.461	0.62	0.825
U^* (exptl)	0.453	0.507	0.613	0.993
% deviation	−9.5	−9.3	0.82	−16.9

In each subproblem, the particle experiences an electrical force, $\mathbf{F}_e$, and a hydrodynamic force, $\mathbf{F}_d$. If we let F_{ei} and F_{di} be the magnitudes of $\mathbf{F}_e$ and $\mathbf{F}_d$ in subproblem i, then[33,35]

$$F_{ei}^* = \iint_{S^*} \left[\frac{\partial \psi_e^*}{\partial n} \frac{\partial \delta\psi^*}{\partial z^*} - \left(\frac{\partial \psi_e^*}{\partial t} \frac{\partial \delta\psi^*}{\partial t} \right) n_z \right] \mathrm{d}S^* \tag{39}$$

$$F_{di}^* = \iint_{S^*} (\sigma_{\mathbf{H}}^* \cdot \mathbf{n}) \cdot \mathbf{e}_z \, \mathrm{d}S^* \tag{40}$$

where $F_{ei}^* = F_{ei}/\varepsilon\zeta^2$ and $F_{di}^* = F_{di}/\varepsilon\zeta^2$ are the scaled electric force and the scaled hydrodynamic force, respectively, acting on the particle in the ith subproblem. $S^* = S/a^2$ is the scaled surface area, with S being the particle surface area; n and t are the magnitude of the unit normal vector and that of the unit tangential vector, respectively; n_z is the z-component of n; $\sigma_{\mathbf{H}}^* = \sigma_{\mathbf{H}}/(\varepsilon\zeta^2/a^2)$ is the scaled shear stress tensor, with $\sigma_{\mathbf{H}}$ being the shear stress tensor.

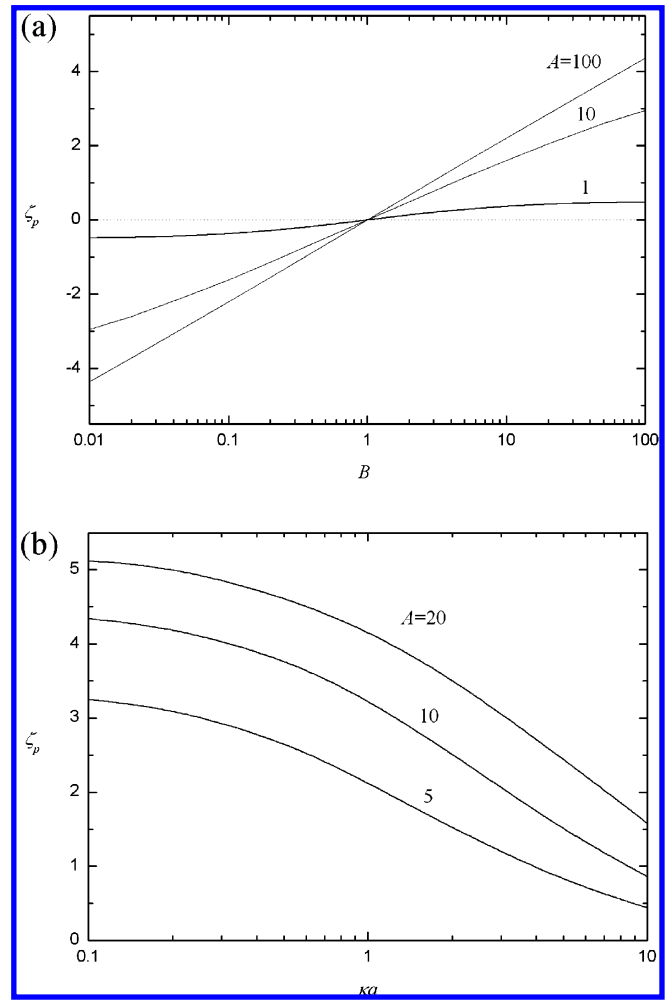

Figure 4. Variations of the scaled surface potential ζ_p of the particle as a function of (a) parameter B and (b) κa for various levels of A. (a) $\kappa a = 1$, (b) $B = 100$ and $\omega = 0.1$.

3. Results and Discussion

FlexPDE,[36] a finite-element-based software, is adopted to solve the present boundary-valued problem; a detailed solution procedure can be found in the literature.[27,28] Grid independence is checked throughout the computation. Using a total of ~5000 and 8000 nodes is usually sufficient for the resolution of the flow field and the electric field, respectively. Figure 2 shows the typical mesh structure on the half plane $\theta = \pi/2$ for the case that the number of nodes is 5569.

The applicability of the software adopted is also justified by using it to solve the diffusiophoresis of an isolated, rigid sphere under the conditions of low surface potential,[37] where an analytical solution was derived. Figure 3 shows the variation of the scaled diffusiophoresis mobility of a particle, $U^* = U/U_{ref}$, as a function of the scaled surface potential ζ_p. Both the present numerical results and the corresponding analytical results[37] are presented. As seen, these results are in good agreement for the range of ζ_p considered. The deviation at large $|\zeta_p|$ is expected because the analytical results are valid for low $|\zeta_p|$ only.

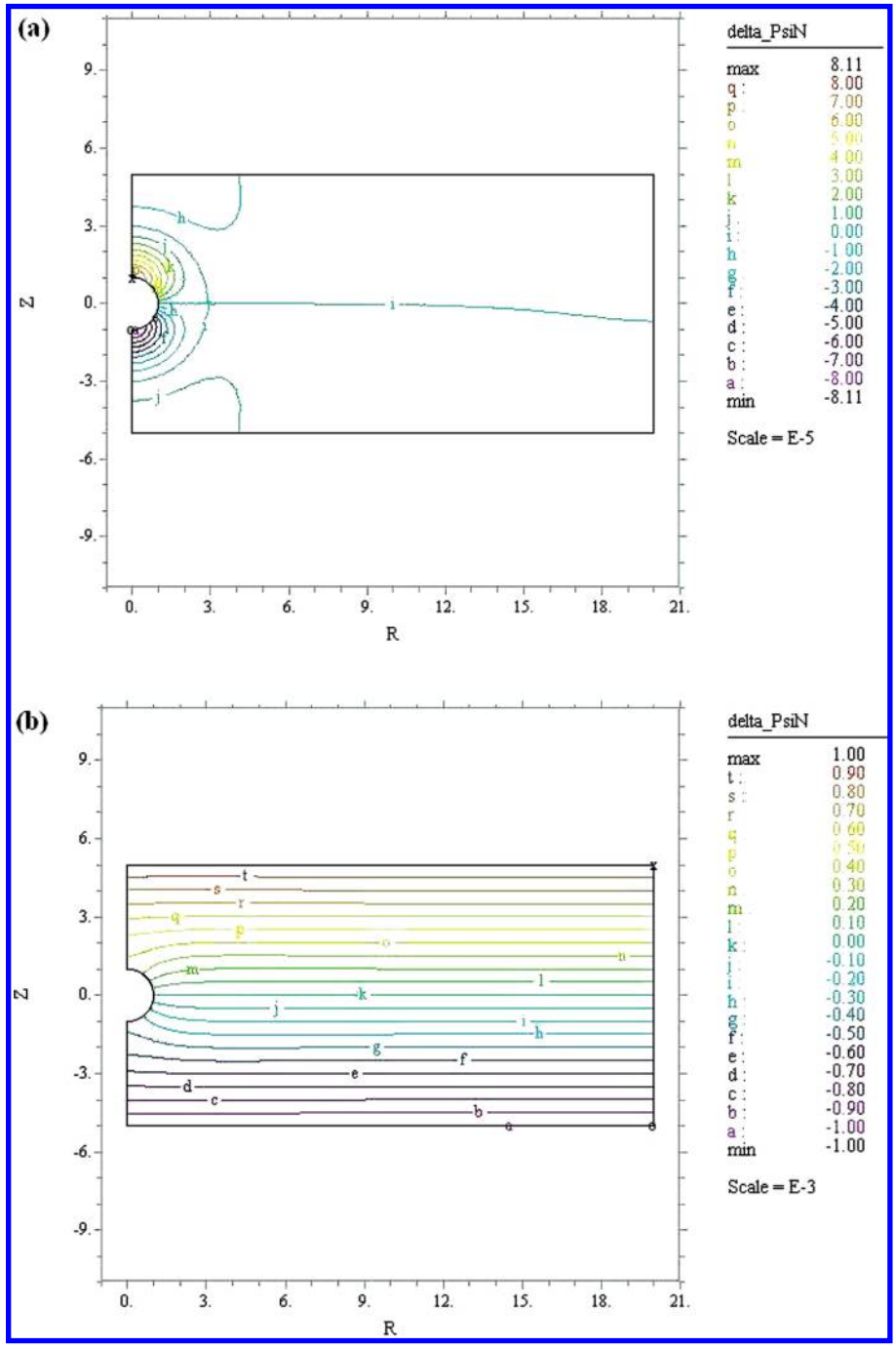

Figure 5. Contours of the scaled perturbed electric potential $\delta\psi^*$ on the half plane $\theta = \pi/2$ at $\kappa a = 1$, $A = 1$, and $B = 0.01$, where $Z = z/a = z^*$ and $R = r/a$. (a) $\beta = 0$ and (b) $\beta = -0.2$.

The applicability of the present theoretical model is examined by fitting it to the available experimental data in the literature. To this end, the results of Ebel et al.[10] are chosen, in which the diffusiophoresis of dilute polystyrene latex spheres was conducted. In the data-fitting procedure, a large value is assumed for A (>1000) so that the surface potential remains at a constant level, and the values of B, ω, and θ are adjusted to fit the surface potential in the experiment. In addition, a small value of λ (<0.3) is used to simulate the dilute condition. Table 1 summarizes the results obtained. Due to the limitation of the numerical procedure adopted, only the results for $\kappa a < 30$ are presented. Table 1 reveals that the agreement between the results based on the present theoretical model and those observed experimentally is reasonably good.

The diffusiophoretic behavior of a particle under various conditions is examined through varying the values of the parameters that are key to the system under consideration. Unless otherwise specified, we assume $\gamma = 10^{-3}$, $\alpha = 1$, $\omega = 1$, $\theta = 1$, $\lambda = 0.2$, and $P = 0\%$, where $P = 100\% \times m/(b - a)$. Two representative types of aqueous electrolyte solution are considered: namely, KCl ($Pe_1 = Pe_2 = 0.26$, $\beta = 0$) and NaCl ($Pe_1 = 0.39$, $Pe_2 = 0.26$, $\beta = -0.2$).[16,34] For illustration, we assume that the disks are uncharged.

Influences of Parameters A, B, and κa on Surface Potential. Figure 4 illustrates the variation of the scaled surface potential ζ_p of a particle under various conditions at $\lambda = 0.2$ and $P = 0\%$, where the presence of the disks is relatively unimportant. This figure reveals that $|\zeta_p|$ increases with increas-

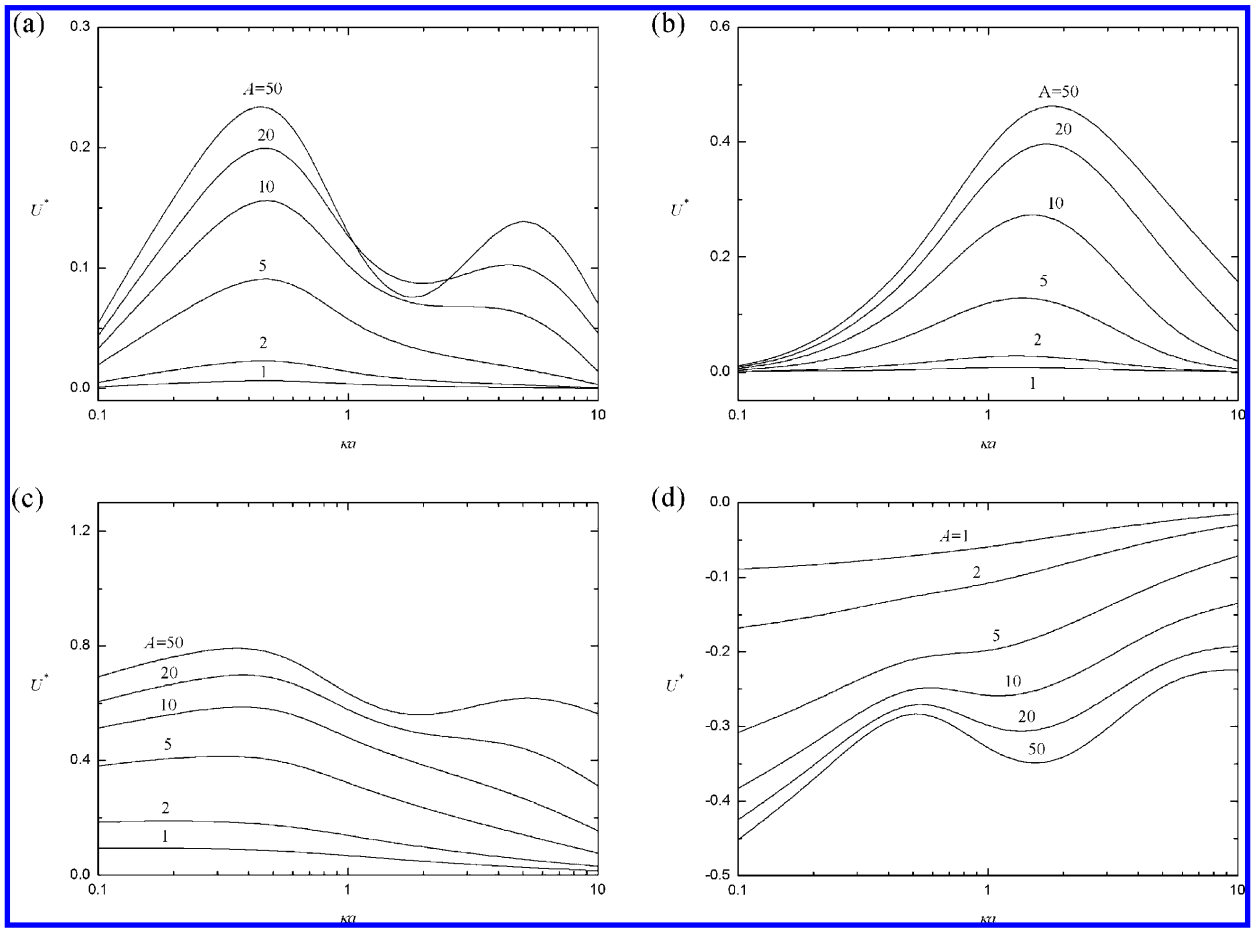

Figure 6. Variations of the scaled diffusiophoresis mobility U^* as a function of κa at various combinations of A, B, ω, β, and λ. (a) $\zeta_p < 0$, $\beta = 0$, $\lambda = 0.2$; (b) $\zeta_p < 0$, $\beta = 0$, $\lambda = 0.5$; (c) $\zeta_p < 0$, $\beta = -0.2$, $\lambda = 0.2$; (d) $\zeta_p > 0$, $\beta = -0.2$, $\lambda = 0.2$. $B = 0.01$ and $\omega = 10$ for $\zeta_p < 0$, and $B = 100$ and $\omega = 0.1$ for $\zeta_p > 0$.

ing A. This is reasonable because A is a measure for the number concentration of the dissociable acidic functional groups, and a larger A yields a larger $|\sigma_p^*|$ and, therefore, a higher $|\zeta_p|$. According to eqs 18 and 19, an increase in $[H^+]_0$ (or B) drives the reactions to the left, yielding an increase in the amount of positive charge on the particle surface. On the contrary, a smaller value of B results in less negative charge on the particle surface. Therefore, both a large and a small value of B yield a large $|\zeta_p|$, as seen in Figure 4a. Note that if $B = 1$, $[Q_A^-]_s = [Q_BH^+]_s$; that is, the particle surface is neutral. Figure 4b shows that ζ_p (or $|\zeta_p|$) decreases with increasing κa. This is because as κa increases (thickness of double layer decreases), $|\sigma_p^*|$ increases, but $|\zeta_p|$ decreases simultaneously, and the effect of the latter is more important than that of the former. Therefore, the thinner the double layer, the smaller the $|\zeta_p|$. A similar phenomenon is also observed in the literature.[33,38]

Types I and II DLP. Figure 5 illustrates the contours of the scaled perturbed electric potential, $\delta\psi^*$, at two levels of β. As shown in Figure 1, the ionic concentration in the top region of the particle is higher than that in the bottom region of the particle. In the present case, because $B < 1$, the particle is negatively charged. With the applied concentration gradient, the perturbed concentration of counterions (cations) inside the double layer in the top region of the particle is higher than that in the bottom region of the particle. This induces a local electric field, which drives a particle, regardless of the sign of its charge, toward the high-concentration side (upward). As seen in Figure 5a, the higher ionic concentration in the top region of the particle leads to a positive $\delta\psi^*$ inside the double layer on the high concentration side and a negative $\delta\psi^*$ inside the double layer on the low concentration side. This phenomenon is defined as type I DLP,[16] which yields an upward electric force acting on the particle. As indicated by Figure 5a, $\delta\psi^*$ becomes slightly negative outside the double layer in the top region of the particle, implying that the perturbed concentration of co-ions outside the double layer in the top region of the particle is higher than that of counterions. This phenomenon is defined as type II DLP,[16] which reduces the upward electric force acting of the particle coming from type I DLP. In general, type I DLP is more important than type II DLP; that is, chemiphoresis usually drives a particle toward the high concentration side (upward).

The distribution of $\delta\psi^*$ on the low concentration side of the particle is similar to that on the high concentration side of the particle, but with opposite sign. This implies that the perturbed concentration of co-ions is higher than that of counterions inside the bottom region of the double layer, but the perturbed concentration of counterions is higher than that of co-ions outside the bottom region of the double layer. Figure 5b reveals that for the case that $\beta = -0.2$, the difference between the diffusivity of cations and that of anions yields a background electric field, which drives a negatively charged particle upward, known as the electrophoresis effect. For a positively charged particle, although the roles that types I and II DLP play are the same as those for a negatively charged particle, the effect of electrophoresis drives the particle toward the low-concentration side (downward). Therefore, the direction of diffusiophoresis depends on the relative magnitudes of forces coming from type I DLP, type II DLP, and electrophoresis.

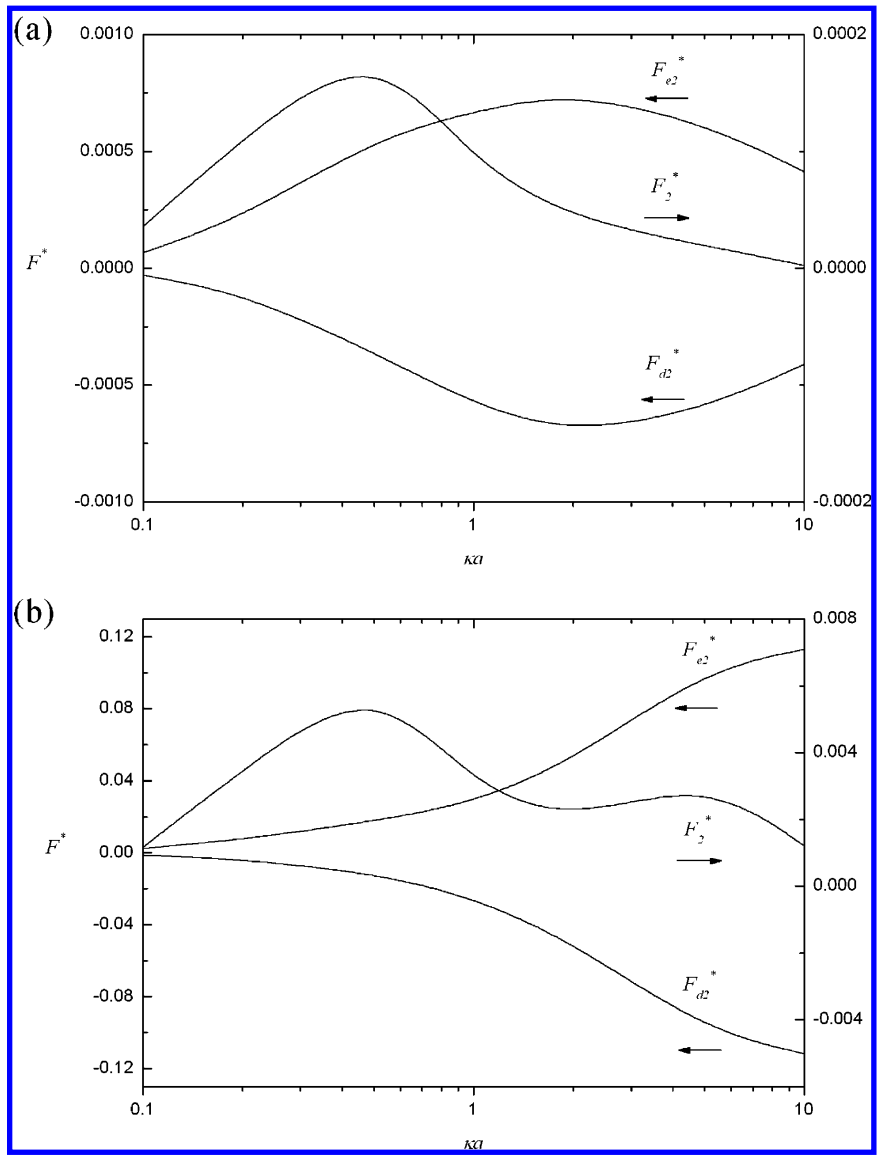

Figure 7. Variations of the scaled forces $F_{\hat{e}2}^*$, $F_{\hat{d}2}^*$, and $F_2^* = F_{\hat{e}2}^* + F_{\hat{d}2}^*$ as a function of κa for the case when $\zeta_p < 0$, $\beta = 0$, and $\lambda = 0.2$. (a) $A = 1$; (b) $A = 20$.

Figure 6 shows the simulated variations of the scaled diffusiophoresis mobility, U^*, as a function of κa at various combinations of A ($= e^2 N_A a/\varepsilon k_B T$), B ($= [H^+]_s/K_A$), ω ($= N_A/N_B$), β ($= (D_1 - D_2)/(D_1 + \alpha D_2)$), and λ ($= a/b$). In Figure 6a, the particle is negatively charged, the effect of electrophoresis is absent ($\beta = 0$), and the boundary effect is relatively unimportant ($\lambda = 0.2$). This figure reveals that the qualitative behavior of U^* as κa variation depends highly on the level of A, which measures the density of the acidic functional groups on the particle surface. If A is smaller than ~10, U^* has a local maximum as κa varies. This is because for small values of κa (thicker double layer), an increase in κa means a higher bulk ionic concentration and, therefore, a more significant type I DLP. On the other hand, for larger values of κa, an increase in κa not only enhances type II DLP but also reduces type I DLP simultaneously, yielding a smaller U^*.

This can be justified in Figure 7a, where the variations of the scaled forces $F_{\hat{e}2}^*$, $F_{\hat{d}2}^*$, and F_2^* ($= F_{\hat{e}2}^* + F_{\hat{d}2}^*$) as a function of κa are presented. Note that the scaled hydrodynamic force $F_{\hat{d}2}^*$ comes mainly from the chemiosmosis caused by type I DLP. If κa is very small, there is no room for type II DLP to takes place. If κa exceeds ~0.5, type II DLP begins to be important, leading to a decrease in $F_{\hat{e}2}^*$. Therefore, the value of κa at which the local maximum of F_2^* occurs is smaller than that of $F_{\hat{e}2}^*$ and that of $|F_{\hat{d}2}^*|$. It is interesting to see in Figure 6a that if A exceeds ~10, U^* has another local maximum at $\kappa a \cong 5$, which can be explained by Figure 7b. As in the case of Figure 7a, type II DLP begins to be important when κa exceeds ca. 0.5, leading to the first local maximum. As κa increases further, the higher ionic concentration leads to a greater electric repulsive force between the particle and co-ions and, therefore, a more significant type I DLP. For κa ranges from 1 to 5, the increase in the degree of type I DLP is larger than that of type II DLP, yielding the second local maximum.

If the boundary effect is sufficiently important, as in the case of Figure 6b, the second local maximum disappears. This is because if the particle is sufficiently close to the disk, the decrease in the space between the outer boundary of the double layer and the disk makes type II DLP stronger, and it becomes more significant than type I DLP. A comparison between Figure 6a and c reveals that, due to the presence of the effect of electrophoresis in the latter, the U^* of a negatively charged particle for the case when $\beta = -0.2$ is much larger than that for the case when $\beta = 0$. This is consistent with experimental

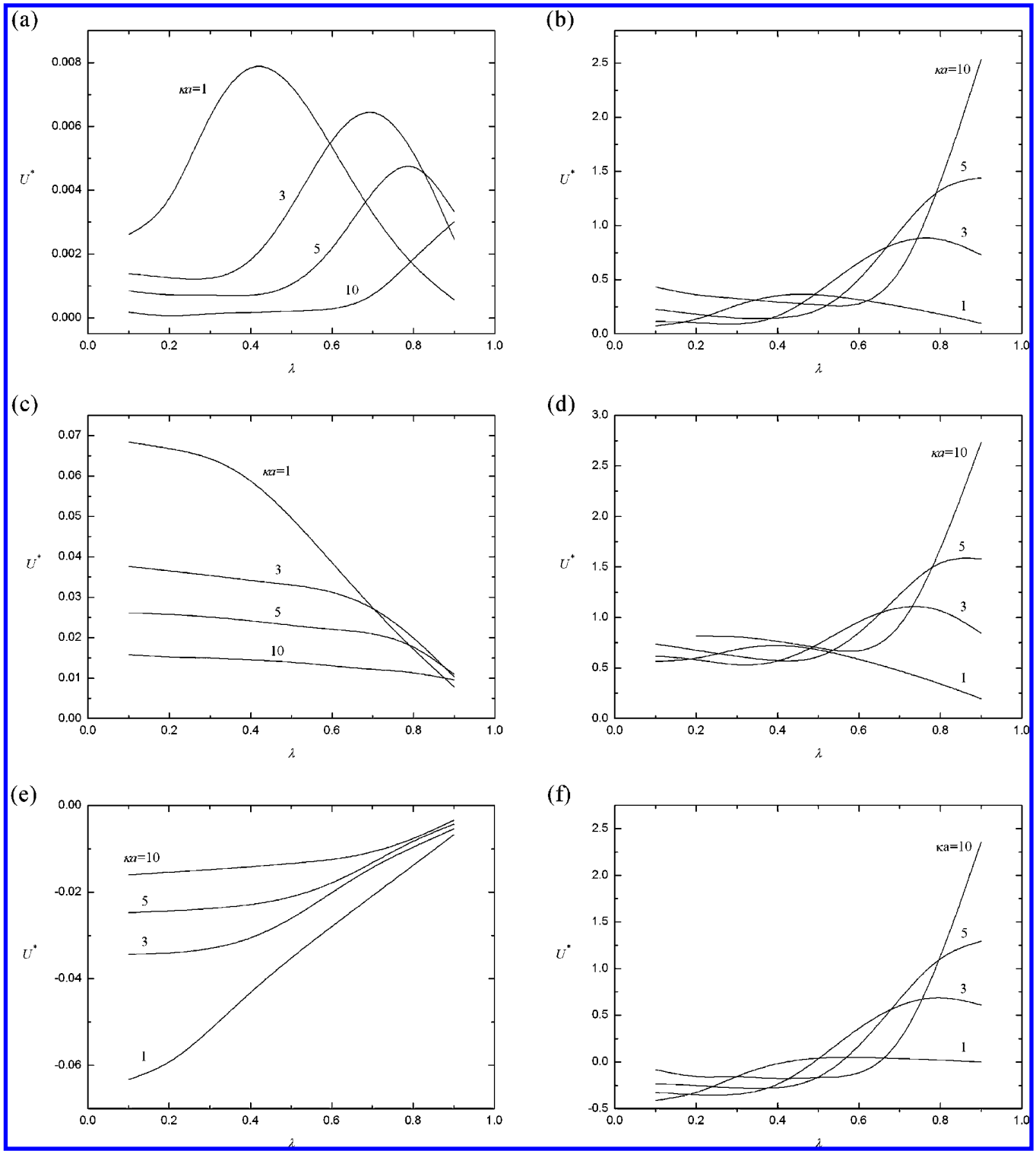

Figure 8. Variations of the scaled diffusiophoresis mobility U^* as a function of λ at various combination of κa, A, B, and β. (a) $A = 1$, $\zeta_p < 0$, $\beta = 0$; (b) $A = 100$, $\zeta_p < 0$, $\beta = 0$; (c) $A = 1$, $\zeta_p < 0$, $\beta = -0.2$; (d) $A = 100$, $\zeta_p < 0$, $\beta = -0.2$; (e) $A = 1$, $\zeta_p > 0$, $\beta = -0.2$; (f) $A = 100$, $\zeta_p > 0$, $\beta = -0.2$. $B = 0.01$ for $\zeta_p < 0$, and $B = 100$ for $\zeta_p > 0$.

observations.[10] On the other hand, as seen in Figure 6d, the mobility of a positive particle becomes negative; that is, it moves toward the low-concentration side (downward). Figure 6c and d suggest that if A is not large, $|U^*|$ decreases with increasing κa. This is because the larger the κa (higher ionic concentration and thinner double layer), the stronger the electroosmotic retardation flow, and the closer it is to the particle. However, if A is sufficiently large, the significance of the effect of chemiphoresis is comparable to that of electrophoresis, and therefore, $|U^*|$ has two local maximums.

Influence of Boundary. The influence of the boundary effect on the diffusiophoretic behavior of a particle under various conditions is illustrated in Figure 8. In Figure 8a and b, $\beta = 0$ (that is, the effect of electrophoresis is absent), but that effect is present in Figure 8c−f, where $\beta = -0.2$. As seen in Figure 8a, U^* has a local maximum as λ varies, and the value of λ at which the local maximum occurs increases with increasing κa. This is because the occurrence of the local maximum is caused mainly by the presence of the boundary; the thinner the double layer, the shorter the particle−boundary distance that is neces-

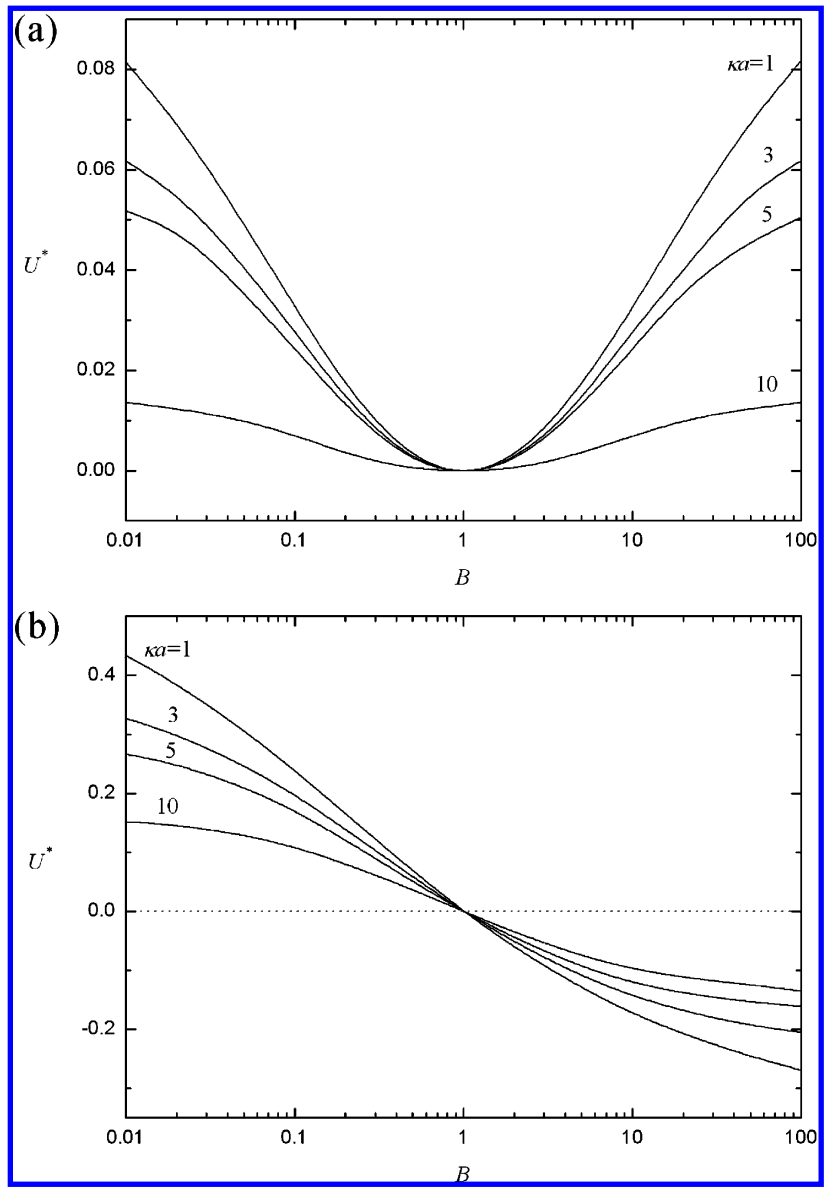

Figure 9. Variations of the scaled diffusiophoresis mobility U^* as a function of parameter B at various combinations of κa and β at $A = 10$. (a) $\beta = 0$; (b) $\beta = -0.2$.

sary for the boundary effect to be significant. In other words, the largest U^* occurs when the boundary is slightly outside the double layer, because in that case, there is not enough room for type II DLP to take place. If the particle−boundary distance is further decreased, the hydrodynamic drag dominates, leading to a decrease in U^*. Note that, due to the effect of type II DLP, U^* decreases with increasing κa for smaller values of λ. The value of A in Figure 8b is larger than that in Figure 8a, leading to a larger U^*. Other than that, the qualitative behaviors of U^* in these two figures is similar. If the particle is close to the boundary, the value of U^* at large κa becomes very large. This is because type I DLP dominates in the present case of highly charged particle surface.

If the effect of electrophoresis is present, such as in Figure 8c and e, where A is small, the behavior of U^* is less complicated than that seen in Figure 8a. In this case, the larger the λ, the smaller the $|U^*|$, and if λ is not too large, the larger the κa, the smaller the $|U^*|$. The former arises because the larger the λ, the greater the hydrodynamic drag as a result of the boundary acting on the particle. The latter arises from the electroosmotic retardation flow, as discussed in Figure 6c and d. Figure 8a, c, and e reveals that if the surface charge density is low, varying the value of β and the sign of the fixed charge on the particle surface leads to an appreciable change in U^*, but that change becomes limited if the surface charge density is high. This implies that if the surface charge density is low, the effect of electrophoresis is more significant than that of chemiphoresis, and the reverse is true if it is high. Figure 8f indicates that if a positively charged particle is sufficiently close to a boundary, its mobility may change the sign from negative to positive. As can be inferred from Figure 8b, where the effect of electrophoresis is absent, this arises from the enhancement of the effect of chemiphoresis. Figure 8b, d, and f suggests that the effect of electrophoresis is more significant at small values of λ. This is because the increase in $|U^*|$ due to the electrophoresis effect is hindered by the strong hydrodynamic drag coming from the presence of the boundary at a large λ.

Influence of Parameter B. Figure 9 shows the influence of parameter B, which measures the bulk concentration of H^+, on the scaled diffusiophoretic mobility, U^*. The effect of electrophoresis is absent in Figure 9a. In this case, if a particle is positively charged ($B > 1$), U^* increases with increasing B and

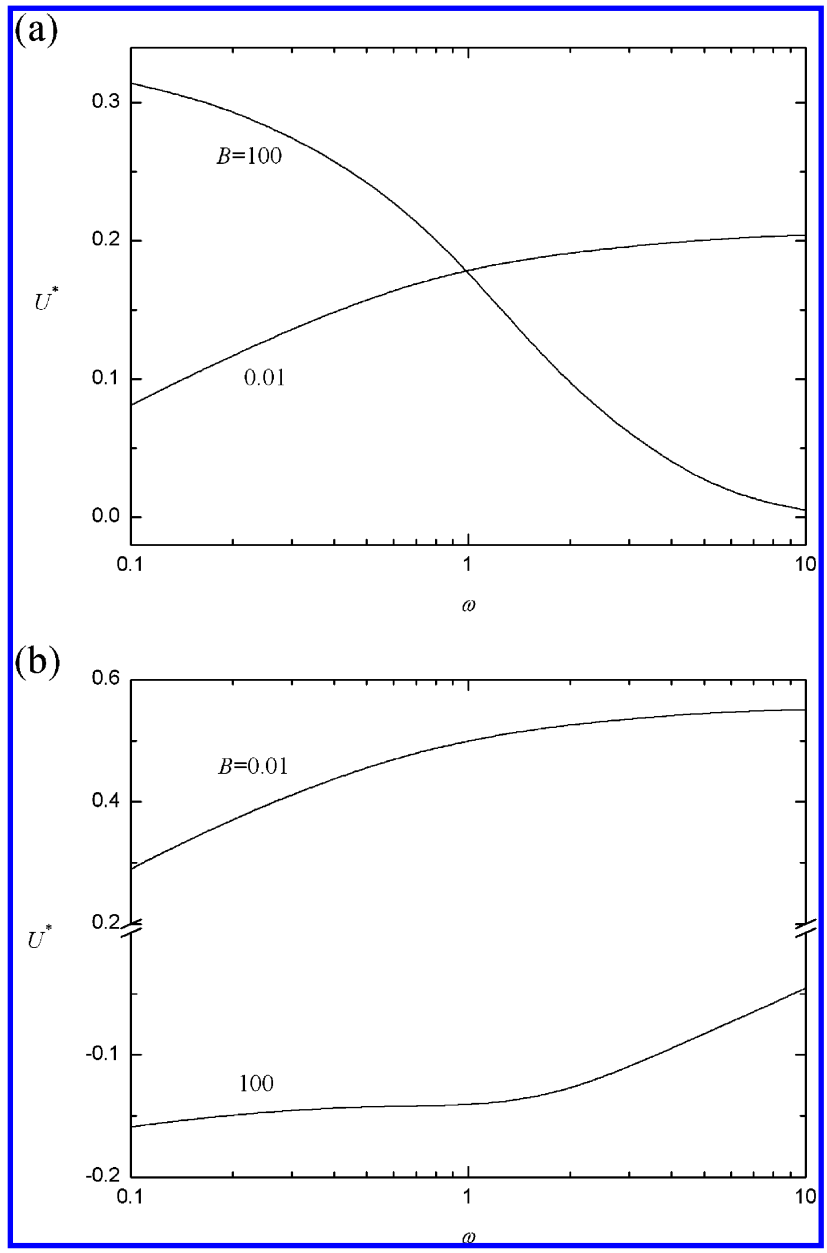

Figure 10. Variations of the scaled diffusiophoresis mobility U^* as a function of ω ($= N_A/N_B$) at various combinations of B and β at $A = 10$, $\lambda = 0.3$, and $\kappa a = 1$. (a) $\beta = 0$; (b) $\beta = -0.2$.

decreases with increasing B if it is negatively charged ($B < 1$). The former is because the larger B implies a higher $[H^+]_0$, a smaller K_A, or both, leading to a higher $[Q_BH^+]_s$ and a lower $[Q_A^-]_s$ from Le Chatelier's principle, and the latter can be explained by similar reasoning. These behaviors are consistent with the results shown in Figure 4a. The curves in Figure 9a are symmetric about $B = 1$. This is because in the case of chemiphoresis, U^* is dependent on the density of the fixed charge on the particle surface but is independent of its sign. Figure 9a also shows that due to the presence of type II DLP, U^* decreases with increasing κa.

The effect of electrophoresis is present in Figure 9b. In this case, the induced background electric field arising from the difference in the diffusivities of cations and anions drives a negatively charged particle toward the high-concentration side and a positively charged particle toward the low-concentration side. Here, $|U^*|$ is seen to increase with increasing B for $B > 1$, and increases with decreasing B for $B < 1$. This is expected because the magnitude of U^* depends upon the charge density on the particle surface. Note that although the electrophoresis effect dominates the direction of diffusiophoresis, due to the presence of the chemiphoresis effect, $|U^*(B < 1)| > |U^*(B > 1)|$.

Influence of Parameter ω. The influence of parameter ω ($= N_A/N_B$), which measures the relative magnitudes of the surface concentrations of the acidic and the basic functional groups, on the diffusiophoretic behavior of a particle, is shown in Figure 10. Figure 10a, where $\beta = 0$, suggests that the qualitative behavior of the scaled mobility, U^*, as ω varies depends upon the magnitude of B (or the sign of the charged conditions on the particle surface). For a fixed value of A, an increase in ω yields a smaller N_B, and therefore, a lower $[Q_BH^+]_s$, as can be inferred from eqs 22 and 23. In this case, if the particle is positively charged ($B = 100$), $|\zeta_p|$ decreases with increasing ω, as does U^*. On the other hand, if the particle is negatively charged ($B = 0.01$), $|\zeta_p|$ increases with increasing ω, as does U^*. As seen in Figure 10b, where $\beta = -0.2$, $|U^*|$ decreases with increasing ω if the particle is positively charged

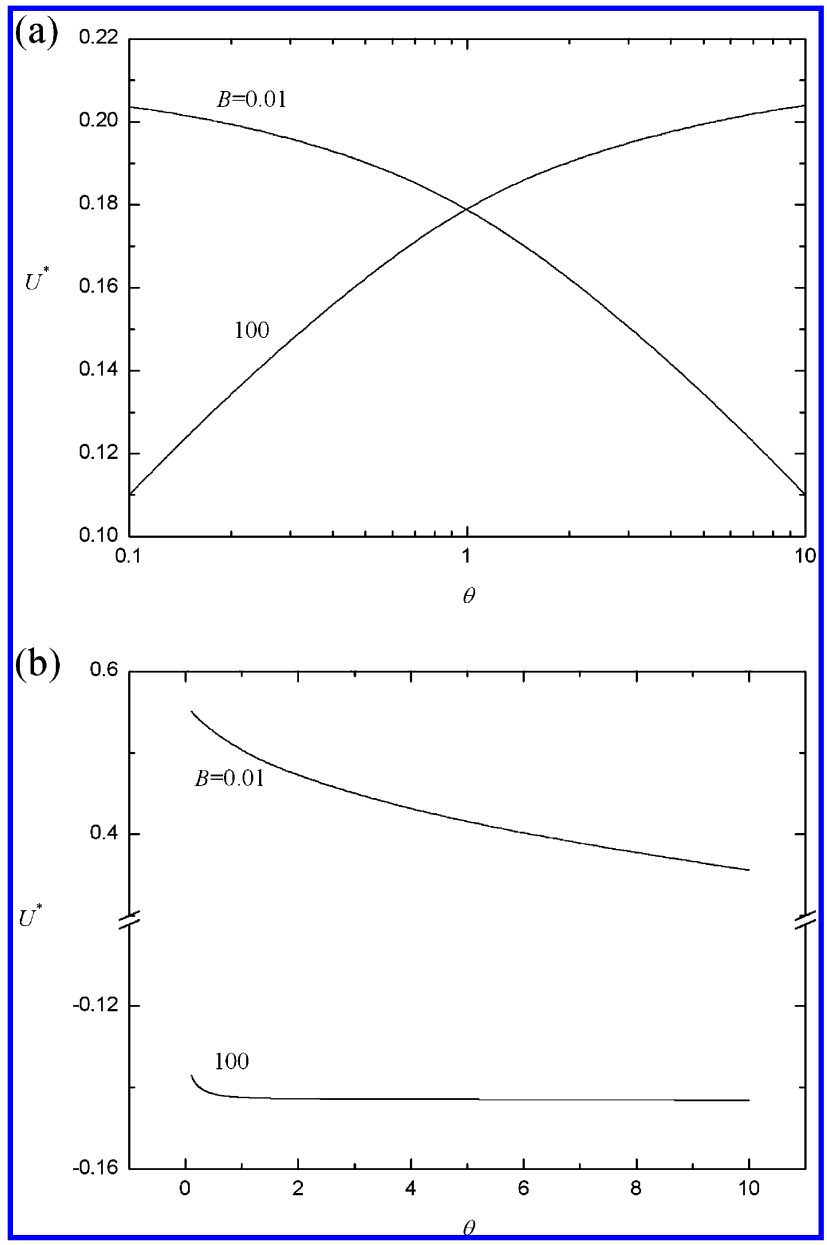

Figure 11. Variations of the scaled diffusiophoresis mobility U^* as a function of θ ($= K_A/K_B$) at various combination of B and β at $A = 10$, $\lambda = 0.3$, and $\kappa a = 1$. (a) $\beta = 0$; (b) $\beta = -0.2$.

($B = 100$), but the opposite trend is observed if the particle is negatively charged ($B = 0.01$). This is because an increase in ω yields a decrease in $[Q_BH^+]_s$. To an originally negatively charged particle, this leads to a larger absolute value of the total amount of fixed charge and a smaller absolute value of the total amount of fixed charge to an originally positively charged particle.

Influence of Parameter θ. Figure 11 shows the influence of parameter θ ($= K_A/K_B$), which measures the relative significance of the dissociation/association reactions expressed in eqs 18 and 19 on the scaled diffusiophoresis mobility, U^*. The qualitative behavior of U^* as θ varies is seen to depend upon the charged conditions on the particle surface. According to Le Chatelier's principle, if A is fixed, an increase in θ implies a decrease in K_B and, therefore, an increase in $[Q_BH^+]_s$ according to eq 19. Figure 11a indicates that for a positively charged particle ($B = 100$), an increase in θ leads to an increase in U^*, but that trend becomes reversed for a negatively charged particle. As seen in Figure 11b, $|U^*|$ decreases with increasing ω for a positively charged particle, but increases with increasing ω for a negatively charged particle. This is because in this case, an increase in $[Q_BH^+]_s$ implies an increase in the downward electric force coming from the electrophoresis effect acting on the particle.

Influence of Parameter *P*. Figure 12 illustrates the variations of the scaled diffusiophoresis mobility U^* as a function of the position parameter P ($= 100\% \times m/(b - a)$) at various combinations of κa, B, and β for the case when the surface charge density is high ($A = 100$). Here, the larger the value of $|P|$, the closer the particle to one of the disks. As seen in Figure 12a, U^* has a local maximum as the particle approaches one of the two disks. If $|P|$ is large, the compression of the double layer enhances type I DLP and reduces the room available for type II DLP, yielding a large U^*. These can be justified because the thinner the double layer, the larger the value of P at which the local maxima occur; similar results are also found in Figure 8. Note that the nonslip boundary condition assumed on the disks implies that U^* should vanish at $|P| = 100\%$. As illustrated in Figure 12c, the boundary effect plays an important role in

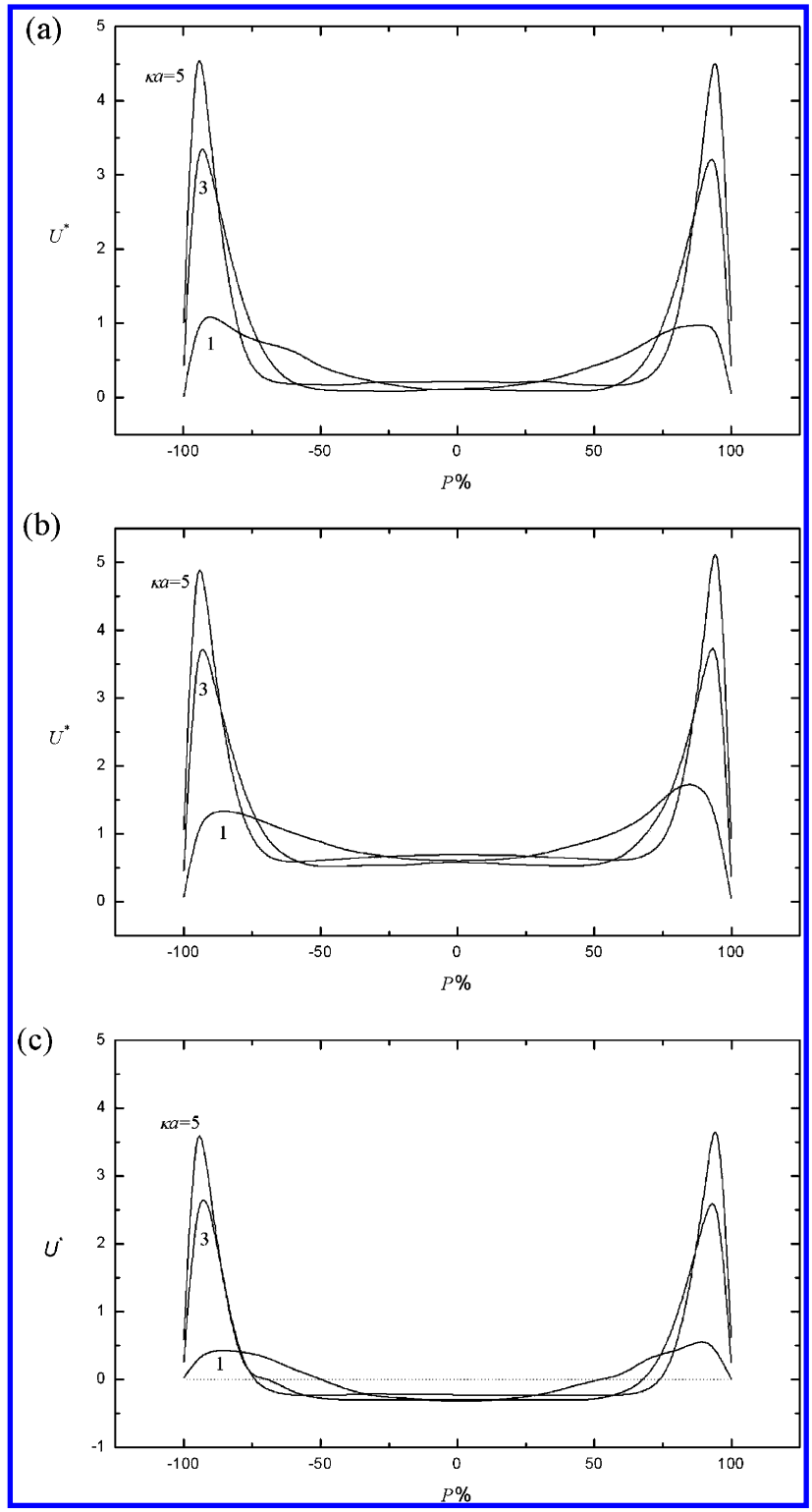

Figure 12. Variations of the scaled diffusiophoresis mobility U^* as a function of position parameter P ($= 100\% \times m/(b - a)$) at various combinations of κa, B, and β at $A = 100$, $\lambda = 0.2$, $\omega = 2$, and $\theta = 2$. (a) $\zeta_p < 0$, $\beta = 0$; (b) $\zeta_p < 0$, $\beta = -0.2$; (c) $\zeta_p > 0$, $\beta = -0.2$. $B = 0.01$ for $\zeta_p < 0$, and $B = 100$ for $\zeta_p > 0$.

diffusiophoresis. For a positively charged particle and $\beta = -0.2$, the direction of diffusiophoresis depends upon the relative significance of chemiphoresis and electrophoresis, two competitive effects. If $|P|$ is not large (particle is away from boundaries), because the electrophoresis effect dominates, the particle moves to the low-concentration side. On the other hand, if the particle is close to the boundaries, because the chemiphoresis effect dominates, it moves to the high-concentration side.

4. Conclusions

In summary, the diffusiophoresis of a charge-regulated spherical particle at an arbitrary position between two large parallel disks is investigated theoretically, taking account of the effects of chemiphoresis and electrophoresis. Here, the surface of the particle carries both acidic and basic functional groups; the dissociation/association of these functional groups yields a

fixed charge. We show that both the chemiphoresis, which comprises two types of double-layer polarization (DLP), and the electrophoresis are affected significantly by the boundary effect, leading to profound diffusiophoretic behaviors. Depending upon the concentration of the functional groups on the particle surface and whether the boundary effect is significant, the diffusiophoretic mobility of the particle can have one or two local maximum as the thickness of double layer varies. If the concentration of the functional groups is low, the electrophoresis effect dominates, and if it is high, the chemiphoresis dominates.

The diffusiophoretic mobility has a local maximum as the particle−boundary distance varies, and the thinner the double layer, the closer the particle−boundary distance at which the local maximum occurs. The more important the boundary effect, the less significant the electrophoresis effect is. The higher the concentration of the functional groups, the larger the absolute value of the diffusiophoretic mobility.

For the case when the diffusivity of cations is the same as that of anions (that is, the electrophoresis effect is absent), we conclude the following: (a) Both a high and a low bulk proton concentration lead to a larger absolute value of the diffusiophoretic mobility. (b) For a positively charged particle, a smaller ratio ω (= dissociation constant of acidic functional groups/dissociation constant of basic functional groups) or a larger ratio θ (= number concentration of acidic functional groups/number concentration of basic functional groups) yields a larger absolute value of the diffusiophoretic mobility. (c) For a negatively charged particle, a larger ω or a smaller θ leads to a larger absolute value of the diffusiophoretic mobility.

For the case when the diffusivity of cations is smaller than that of anions, (that is, the electrophoresis effect is present), we conclude the following: (a) The charge conditions (sign and density) on the particle surface are influenced by the bulk proton concentration. Both a high and a low bulk proton concentration lead to a larger absolute value of the diffusiophoretic mobility. (b) If the direction of diffusiophoresis is toward the high-concentration side, then a larger ω or a smaller θ yields a larger diffusiophoretic mobility. (c) If the direction of diffusiophoresis is toward the low-concentration side, then a smaller ω or a larger θ yields a larger absolute value of the diffusiophoretic mobility. (d) For a positively charged particle, increasing the degree of significance of the boundary effect may result in a change in its direction of diffusiophoresis.

Acknowledgment. This work is supported by the National Science Council of the Republic of China.

References and Notes

(1) Dukhin, S. S.; Deryaguin, B. V. *Surface and Colloid Science*; Wiley: New York, 1974; Vol. 7.
(2) Wei, Y. K.; Keh, H. J. *J. Colloid Interface Sci.* **2004**, *204*, 240.
(3) Keh, H. J.; Wan, Y. W. *Chem. Eng. Sci.* **2008**, *63*, 1612.
(4) Knox, J. H.; McCormick, R. M. *Chromatographia* **1994**, *38*, 207.
(5) Bakanov, S. P.; Vysotskii, V. V. *Colloid J. USSR* **1991**, *53*, 663.
(6) Dvornichenko, G. L.; Nizhnik, Y. V.; Slavikovskii, T. V. *Colloid J. Russ. Acad. Sci.* **1993**, *55*, 36.
(7) Zoulalian, A.; Albiol, T. *Can. J. Chem. Eng.* **1998**, *76*, 799.
(8) Munoz-Cobo, J. L.; Pena, J.; Herranz, L. E.; Perez-Navarro, A. *Nucl. Eng. Des.* **2005**, *235*, 1225.
(9) Carstens, J. C.; Martin, J. J. *J. Atmos. Sci.* **1982**, *39*, 1124.
(10) Ebel, J. P.; Anderson, J. L.; Prieve, D. C. *Langmuir* **1988**, *4*, 396.
(11) Dukhin, S. S.; Martin, E. S.; Dukhin, A. S. *Colloid J. USSR* **1978**, *40*, 536.
(12) Dukhin, S. S.; Martin, E. S.; Dukhin, A. S. *Colloid J. USSR* **1979**, *41*, 734.
(13) Prieve, D. C.; Anderson, J. L.; Ebel, J. P.; Lowell, M. E. *J. Fluid Mech.* **1984**, *148*, 247.
(14) Prieve, D. C.; Roman, R. *J. Chem. Soc., Faraday Trans. II* **1987**, *83*, 1287.
(15) Pawar, Y.; Solomentsev, Y. E.; Anderson, J. L. *J. Colloid Interface Sci.* **1993**, *155*, 488.
(16) Hsu, J. P.; Hsu, W. L.; Chen, Z. S. *Langmuir* **2009**, *25*, 1772.
(17) Wei, Y. K.; Keh, H. J. *J. Colloid Interface Sci.* **2002**, *248*, 76.
(18) Lou, J.; He, Y. Y.; Lee, E. *J. Colloid Interface Sci.* **2006**, *299*, 443.
(19) Lou, J.; Lee, E. *J. Phys. Chem. C* **2008**, *112*, 2584.
(20) Keh, H. J.; Hsu, Y. S. *Chem. Eng. Sci.* **2006**, *61*, 3550.
(21) Chang, Y. C.; Keh, H. J. *J. Colloid Interface Sci.* **2008**, *322*, 634.
(22) Hsu, J. P.; Liu, K. L. *J. Chem. Phys.* **2009**, *130*, 194901.
(23) Healy, T. W.; Chan, D.; White, L. R. *Pure Appl. Chem.* **1980**, *52*, 1207.
(24) Hsu, J. P.; Chen, Z. S.; Tseng, S. *J. Phys. Chem. B* **2009**, *113*, 7701.
(25) Cheng, W. L.; He, Y. Y.; Lee, E. *J. Colloid Interface Sci.* **2009**, *335*, 130.
(26) Keh, H. J.; Li, Y. L. *Langmuir* **2007**, *23*, 1061.
(27) Lee, E.; Chu, J. W.; Hsu, J. P. *J. Colloid Interface Sci.* **1998**, *205*, 65.
(28) O'Brien, R. W.; White, L. R. *J. Chem. Soc., Faraday Trans. 2* **1978**, *74*, 1607.
(29) Hunter, R. J. *Foundations of Colloid Science*; Oxford University: Oxford, 1989; Vol. 1.
(30) Hsu, J. P.; Chen, Z. S. *J. Phys. Chem. B* **2008**, *112*, 11207.
(31) Masliyah, J. H.; Bhattacharjee, S. *Electrokinetic Transport Phenomena*, 4th ed.; Wiley: New York, 2006.
(32) Hsu, J. P.; Kuo, C. C.; Ku, M. H. *Electrophoresis* **2008**, *29*, 348.
(33) Hsu, J. P.; Ku, M. H.; Kuo, C. C. *Langmuir* **2005**, *21*, 7588.
(34) Hsu, J. P.; Lou, Z.; He, Y. Y.; Lee, E. *J. Phys. Chem. B* **2007**, *111*, 2533.
(35) Happel, J.; Brenner, H. *Low Reynolds Number Hydrodynamics*; Martinus Nijhoff: Boston, 1983.
(36) *FlexPDE*, Version 4.24; PDE Solutions Inc.: Spokane Valley, WA, 2004.
(37) Keh, H. J.; Wei, Y. K. *Langmuir* **2000**, *16*, 5289.
(38) Loeb, A. L.; Wiersema, P. H.; Overbeek J. Th. G. *The Electric Double Layer around a Spherical Colloid Particle*; MIT: Boston, 1961.

JP907696T